International Journal on Advanced Science Engineering Information Technology

Vol.11 (2021) No. 3
ISSN: 2088-5334

# Effect of Annealing at High Temperatures on Microstructural Formation of 15Cr-25Ni Austenitic Stainless Steel Cast

Syahbuddin[a,*], Parikin[b], Mohammad Dani[b], Salim Mustofa[b], Andon Insani[b], Eddy Agus Basuki[c], Ching An Huang[d]

[a] *Department of Mechanical Engineering, Faculty of Engineering, Universitas Pancasila, Srengseng Sawah, Jakarta 12640 Indonesia*
[b] *Center for Science and Technology of Advanced Materials, National Nuclear Energy Agency, Puspiptek Area, Banten 15314, Indonesia*
[c] *Department of Metallurgical Engineering, Bandung Institute of Technology, Jl. Ganesha No.10, Bandung, Indonesia*
[d] *Department of Mechanical Engineering, Chang Gung University, Taoyuan, Taiwan*
*Corresponding author: [*] syahbuddin@univpancasila.ac.id*

***Abstract*— Microstructure of 15Cr-25Ni Austenite stainless steel (ASS) cast formed at various high temperatures has been investigated in this study. The steel was synthesized from scrap materials containing Cr and Ni elements, respectively, about 15 and 25 wt.%. This steel designed to have high corrosion resistance or high-temperature oxidation is a steel candidate for evaporator materials in a waste incinerator, and their operating temperature is used for annealing temperatures in this study. The variation of annealing temperatures was carried out at temperatures of 400, 600, 800, 950, and 1078°C for a time of 30 minutes. The ASS as-cast and annealed have a similar microstructure dominated by the dendritic structure of γ-FeNi austenite with the crystal structure of the face-centered cubic interdendritic region of a eutectic structure containing free particle zone and $(Fe, Cr)_7C_3$ island compounds. The short dendritic arm spacings for ASS after annealing at temperatures of 400, 600, and 800°C were measured to have about 61.71, 62.11, and 57.85 μm, respectively. By contrast, the longer dendritic arm spacings were obtained after annealing at temperatures of 950 and 1078°C about 70.29 and 197.04 μm, respectively. In addition to higher micro-strains, the short dendritic arm spacings formed after annealing at 400-800° C lead in a relatively higher hardness profile, whereas the longer dendritic arm spacings obtained after annealing at 950 and 1078°C result in a low hardness profile in the ASS.**

***Keywords*— 15Cr-25Ni austenitic stainless steel; high-temperature annealing; SEM-EDX; neutron diffraction.**

*Manuscript received 22 Nov. 2019; revised 30 Aug. 2020; accepted 2 Dec. 2020. Date of publication 30 Jun. 2021.*


## I. INTRODUCTION

Structural materials for high-temperature components are critical for the system's main developments, mostly metal alloys, i.e., steel. For both Ferritic-Martensitic (F/M) steels and Austenitic steels, some improved alloy compositions have been developed and to be developed continuously. Corrosion seems to be most of the problems encountered by the components operating in a high-temperature environment. High-temperature corrosion (HTC) is significant in energy production, engines, and industrial processes. HTC limits the long-life of installations, restricts fuel utilization, and obstructs the development of more economical, environmentally sustainable processes and systems. Several research application areas, including combustion and gasification of biomass and waste, metallic materials for solid oxide fuel cells (SOFC) [1], and materials for industrial processes, have become up-to-date issues. One component of industrial processes that receive much repetitive heat is in the evaporator or steam generator. The evaporator is often found in industries that process liquids through evaporation. An evaporator [2] is a device that can convert whole or part of a liquid solvent into steam and leave only solid or thick liquid before all liquids are converted into steam, such as sugar industry, milk powder, and petroleum processing. In general, the evaporator system consists of three parts: the heat exchanger, the evaporation section (the place where the liquid/liquid boils and then evaporates), and the separator to separate steam from the liquid [3].

By looking for the evaporator system's field condition, it is very appropriate to apply a material that is resistant to high temperatures (at least above the temperature of the liquid-vapor) to build the system. The evaporator consists of a pressure vessel and a heat exchanger system, which is usually made of copper metal (melting point 1038°C) or steel

(melting point 1500°C). Plant and process engineers are finding material selection to be more critical. Where carbon or low-alloy steels once provided satisfactory service. Engineers are finding it necessary to upgrade to more corrosion-resistant materials, such as stainless steel. Stainless steels have been and will continue to be used extensively in evaporator systems in many industries. They provide excellent corrosion resistance to assure long trouble-free equipment operation and prevent contamination of product streams. Stainless steels resist extremes in temperature, providing excellent strength properties from cryogenic lows up to highs of approximately 1143.33°C (2000°F). Stainless steels resist the buildup of scale and deposits on heat exchange surfaces, and they are readily cleaned.

Material engineers in Indonesian National Nuclear Energy Agency (BATAN) have recently successfully synthesized austenitic superalloy steel using local raw materials. The alloy mostly contains 25%Ni and 15%Cr. This type of austenitic steel [4] is a steel candidate for structural components in multipurpose facilities (i.e., high-temperature structural materials). Therefore, the material must have resistance to mechanical loads, high temperature, and corrosion. These are the main aim and the end-wishing of synthesized steels for a reactor.

As reported before, the 15Cr-25Ni austenitic stainless steel showed a superalloy phenomenon about its corrosion resistance [5], mechanical hardness, and tensile-impact strengths. To bring a significant improvement in the materials' corrosion resistance properties should be the primary objective of synthesizing this new austenitic type of materials having both a moderate nickel and low chromium content must be created. This alloy steel is also expected to have particular advantages such as structural materials for high-temperature operations in general applications due to its being easily fabricated and its economic competitiveness.

In order to produce an austenitic alloy with low carbon concentration, non-standard chemical composition was made in a laboratory-scale fabrication process using a casting method [6]. By considering Ni content [7], the steel is assumed as an advanced type over the T91 and the T92 version and would be expected to be applied as a candidate for a nuclear reactor's structural materials.

This research's main objective is mainly to understand the mechanical-, high temperature- and corrosion resistance-properties of the materials that are very important for the particular application in structural reactor components. The relationship between the structure and behavior of materials can be traced, one of which is micro-crystal structures' appearance. Therefore, the microstructural observation of synthesized materials is presented and discussed.

## II. Material and Method

Materials used in this study are 15Cr-25Ni austenitic stainless steel (ASS) synthesized by casting techniques, as explained in the previous report [8], [9]. The ASS was smelted in an induction furnace at an estimated temperature of more than 1300°C. The chemical composition of the ASS was measured by using an optical emission spectrometer (OES). Since their composition is somewhat different from the chemical composition of the stainless steel in the market; thus, it can be categorized as a new type of ASS. The main ingredients are 25.10% Ni and 15.43% Cr, and a small fraction (below 1.00 wt.%) of other constituents is Nb, Sn, Cu, Ti, W, P, S, Mn, C, Si, and V.

TABLE I
Chemical Compositions of 15Cr-25Ni Austenitic Stainless Steel (Wt.%.)

| **Element** | **Fe** | **Ni** | **Cr** | **Mn** | **C** | **Si** | **Nb** |
|---|---|---|---|---|---|---|---|
| | 57.71 | 25.10 | 15.43 | 0.32 | 0.35 | 0.96 | 0.005 |
| **Element** | **Sn** | **Cu** | **Ti** | **W** | **P** | **S** | **V** |
| | 0.005 | 0.005 | 0.002 | 0.001 | 0.02 | 0.01 | 0.02 |

Annealing processes were conducted at various temperatures of 400, 600, 800, 950, and 1078°C for 30 minutes and cooled inside the furnace chamber. The schematic of all annealing processes for the ASS is shown in Fig. 1.

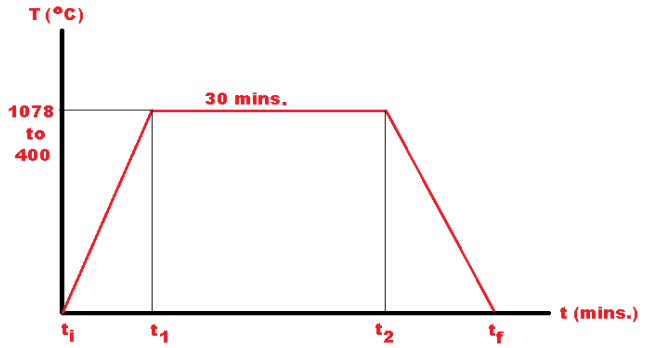


Fig. 1 Annealing processes performed on the ASS at various temperatures of 400, 600, 800, 950 and 1078°C for the time of 30 minutes

Metallographic preparation was performed by cutting, grinding on SiC papers from 220 to 1500 grits, polishing with 1 µm alumina paste and etching in a Kalling reagent solution for 10 seconds to reveal the microstructures of ASS. In order to observe the microstructure and identifying the several phases in the ASS formed after smelting and annealing, an optical microscope (OM) and a scanning electron microscope (SEM, Jeol 2506LV) equipped with energy dispersed X-ray spectrometers (EDXs) were employed. The crystal structure of ASS was investigated using Neutron diffractometer (HRPD).

## III. Results and Discussion

### *A. Matrix of 15Cr-25Ni Austenitic Stainless Steel*

The crystal structure of the ASS was measured using a high-resolution neutron powder diffractometer (HRPD). The neutron diffraction for 15Cr-25Ni austenitic stainless steel samples obtained using HRPD is shown in Figure 2.

The machine was run at a 1.82 Å-wavelengths of neutron thermal at the GA. Siwabessy BATAN reactor in Serpong. The range of diffraction measurements was set from a minimum angular angle of $2\theta = 2.5^{o}$ to a maximum angular angle of $2\theta = 162.5^{o}$. In this study, the as-cast sample was a reference for the other samples annealed at various temperatures of 400, 600, 800, 950, and 1078 °C for the time of 30 minutes. Each diffraction pattern was analyzed by using MAUD software made by Lutterotti [10].

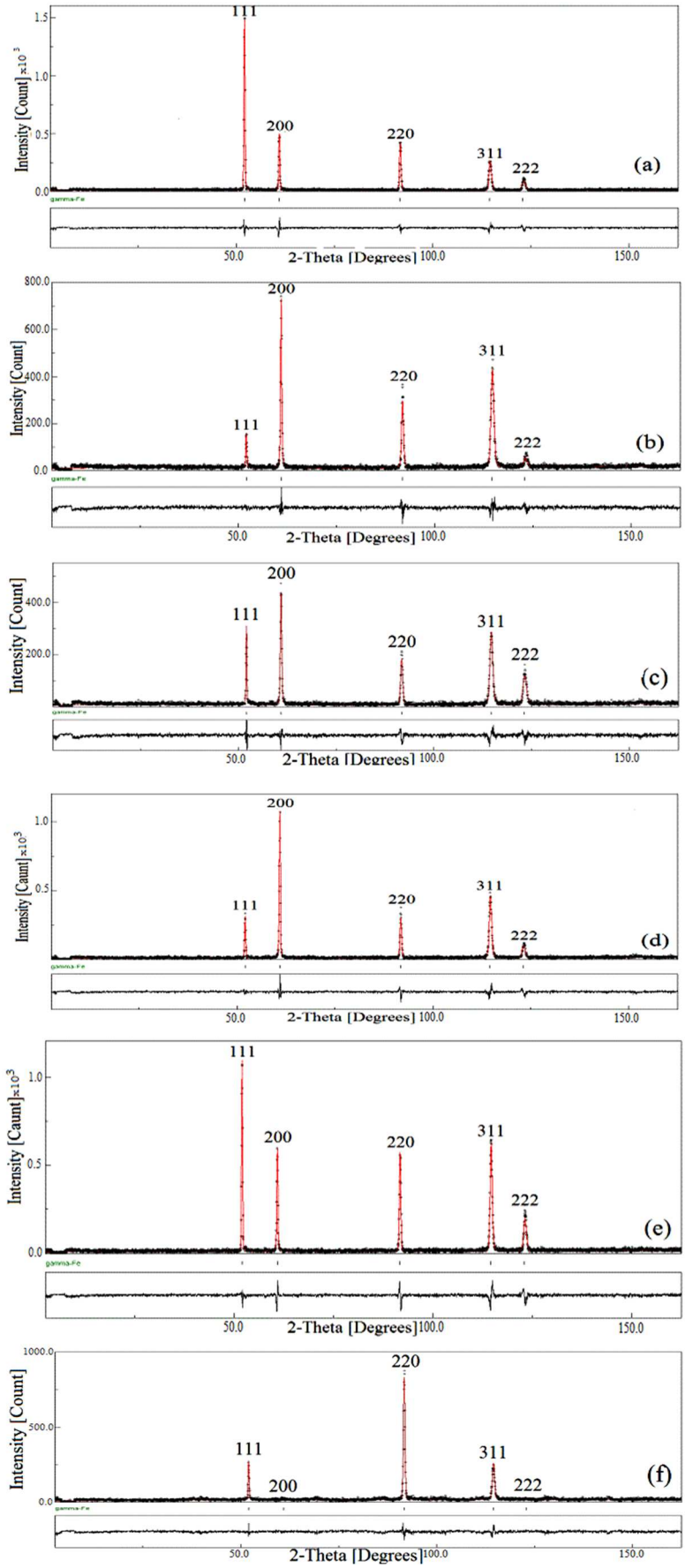


Fig. 2 Neutron diffraction after Rietveld refinements for ASS (a) as-cast, and anealled at (b) 400, (c) 600, (d) 800, (e) 950 and (f) 1087°C

This program was developed to analyze diffraction spectra and obtain crystal structures, quantity, and microstructure of phases along with the texture and residual stresses. Fitting the diffraction spectrum is based on the refinements of the Rietveld method. Profile refinements are fulfilled in the goodness of fits; $\chi^2$ (chi-square) are obtained between 1.3 and 1.4 after convergency is reached. This measurement is found that the austenite phase (γ-Fe) is the dominant phase in this ASS. Five characteristic diffraction peaks for the face centred cubic (I-225) space group are clearly shown in each steel sample, namely: planes of (111), (200), (220), (311) and (222). The lattice parameters of ASS as-cast and annealed is presented in Table 2.

TABLE II
LATTICE PARAMETER OF CRYSTAL STRUCTURE FOR THE ASS AS-CAST AND ANNEALED AT TEMPERATURE OF 400-1078°C FOR 30 MINUTES

| ASS annealed at temperature (°C) | a(Å) | The goodness of fits:$\chi^2$ |
|---|---|---|
| As-Cast | 3.59443 | 1.36 |
| 400 | 3.57470 | 1.34 |
| 600 | 3.58933 | 1.33 |
| 800 | 3.58954 | 1.31 |
| 950 | 3.59182 | 1.35 |
| 1078 | 3.59639 | 1.39 |

During the experiment's execution, the annealing process is predicted to have influenced the orientation of the crystalline plane of the ASS material. Shifting the high intensity of peaks for the diffraction planes was noticed three times. Crystal orientation leads to the peak of (111) diffraction plane or the crystal space's diagonal before the annealing process (as-cast) and when the annealing temperature is about 950 ºC. Turning crystals leading to the dominance of the diffraction peak (200) or in the direction of the coordinate axis (x, y, z) occur at annealing temperatures of 400ºC, 600ºC and 800ºC. As for the annealing temperature of 1078 ºC, the crystal orientation is more directed to the dominance of the diffraction peak of (220) or in the diagonal direction of the crystal plane (x-y, y-z, z-x) and even two peaks of the diffraction plane (200) and (222) sink in the background counts. Therefore, the possibility of orienting the direction of the crystal ASS material is huge during the annealing temperature process (1078ºC)

Figure 3 presented the calculation of lattice parameters for the austenite phase obtained from the ASS as-cast and annealed at temperatures of 400, 600, 800, 950 and 1078°C. The lattice parameter for the ASS as-cast is about 3.5943 Å. After annealing at 400°C, the lattice parameter obtained from the crystal structure is around 3.7947 Å and increases to be 3.5893 Å for annealing at 600°C and 3.5895 Å for annealing 800°C. For higher annealing temperature, the lattice parameters formed are close to the lattice parameter of the ASS as-cast, namely 3.5918 and 3.5963 Å for annealing at temperatures at 950 and 1078°C, respectively. Those lattice parameters close to the lattice parameter of γ-FeNi with a crystal structure of face-centered cubic within the Fm3m space group as reported by several previous studies on austenitic stainless steels [11-13]. Therefore, the ASS matrix is austenitic γ-FeNi. Furthermore, the increase in annealing temperature (from 400 to 1078°C) makes the lattice parameter increases close to the initial lattice parameter of the ASS as-cast.

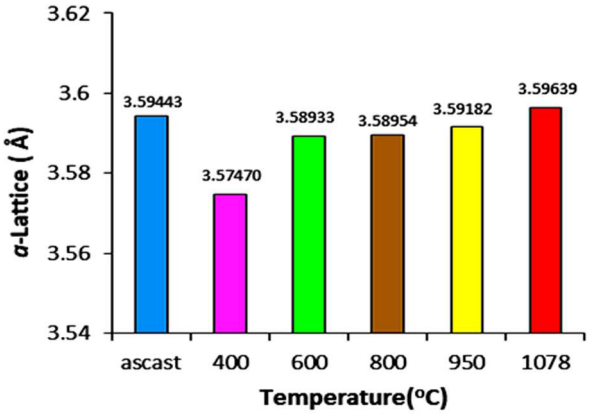


Fig. 3 Lattice parameters of ASS as-cast and annealed at 400-1078°C

*B. Microstructural Formation of 15Cr-25Ni Austenitic Stainless Steel*

As shown in Figure 4, ASS microstructure before and after annealing is dominated by dendrite structure which is characteristic of cast microstructure. Dendrite grains of the γ-Fe phase is surrounded by dendritic boundaries (interdendritic region) which are thought to be composed by the eutectic structure of Fe-Ni-Cr compounds. By using an intersection method, dendrite arm spacing (DAS) for ASS as-cast was calculated to be around 71.70 μm. The DASs annealed at temperatures of 400, 600 and 800°C are fluctuated to be 61.71, 62.11, 57.85 μm. The DAS formed at temperatures of 950 and 1078°C significantly increased to be 70.29 and 197.04 μm, respectively. Such a situation also occurs in the interdendritic region. The region of interdendritic seem to be no differences after annealing at 400, 600, 800°C. However, the region formed at high annealing temperatures at 950 and 1078C is found thicker.

In the following figure (Figure 5) it can be seen that the boundary of FeNiCr eutectic structure as an interdendritic region consists of free particle zone and islands with high C content (grey color), and matrix of α-Fe contains fine particles which tend to accumulate at the edges of dendrites. The particle-free zone's composition was measured 1.33% Si, 17.45% Cr, 55.11% Fe, 26.11% Ni in the ASS as-cast, and 16.36 % Cr, 54.76 % Fe 25.38 % Ni, 3.50 %Ta in the ASS annealed at 1078°C. Similar in the interdendritic region, the composition of islands was 8.29 %C, -63.36% Cr, 1.42 % Mn, 22.31 % Fe and 4.62 % Ni for the ASS as-cast and 7.74 %C, 57.03 %Cr, 1.65 %Mn, 26.03% Fe 7.55% Ni for the ASS annealed at 1078°C. The free particle zones and islands can be considered to have an austenite phase of γ–FeNi and carbide compound (Fe, Cr)7C3, which is also determined by recent studies [14-15]. Fine particles with a composition of 4.45% C, 0.96% Si, 19.74% Cr, 50.62% Fe, 24.53% Ni on the edges of dendrites are estimated as intermetallic compounds of FeNiCr. DAS fluctuations after annealing at 400, 600, and 800°C did not change the thickness of the inter-dendrite region. However, the inter-dendrite region thickens after annealing at 950 and 1078°C. High annealing temperatures increase the size of islands of (Cr, Fe) $_7C_3$ and the number of fine particles of FeNiCr.

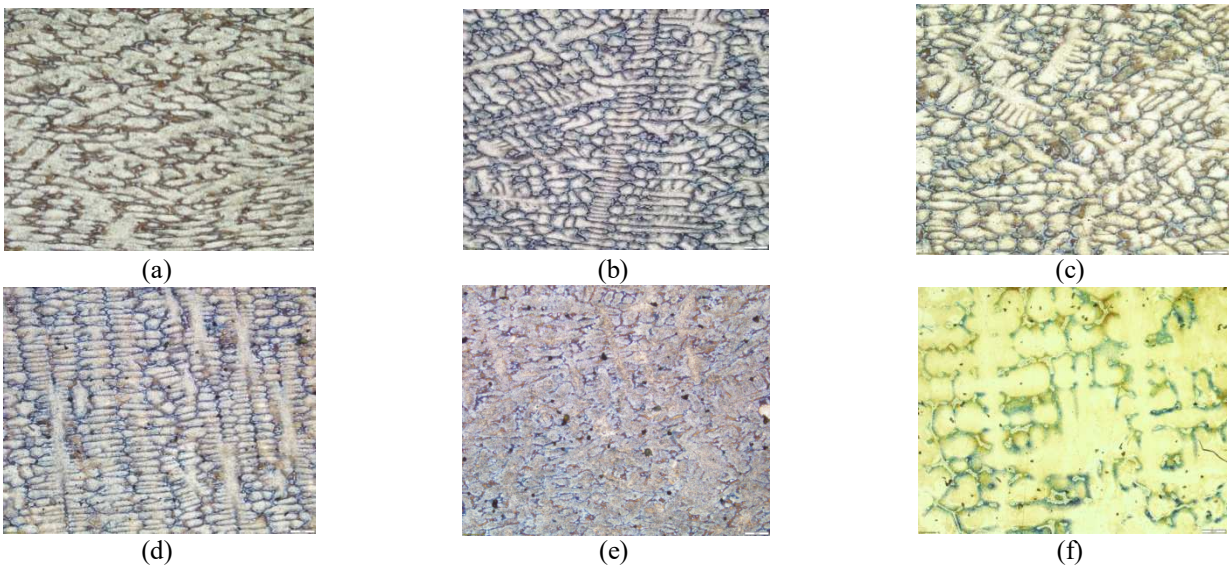


Fig. 4 Microstructure (OM-200x) of ASS samples: (a) as-cast and annealed at (b) 400, (c) 600, (d) 800, (e) 950 and (f) 1078°C

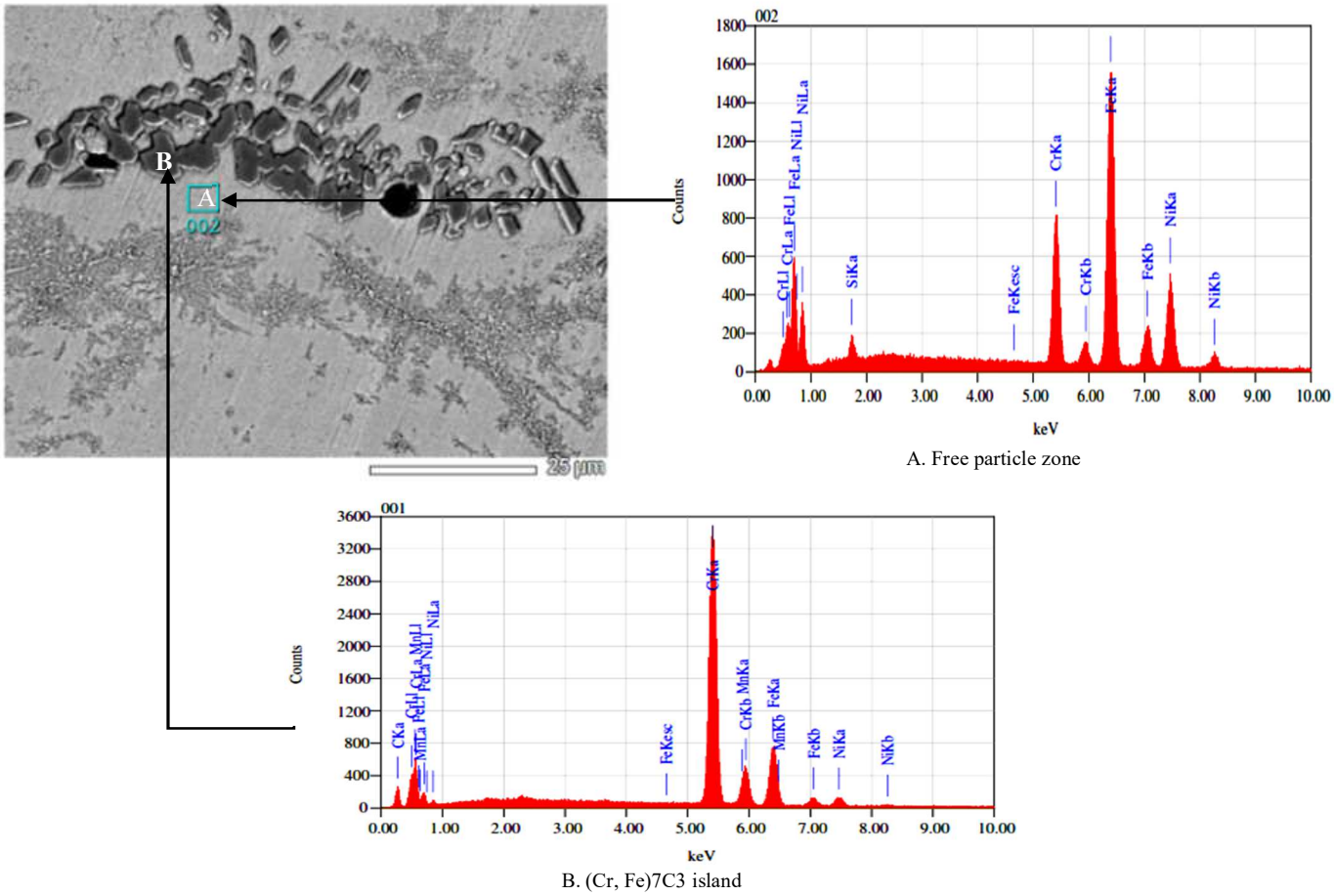


A. Free particle zone

B. (Cr, Fe)7C3 island

a). The ASS as-cast

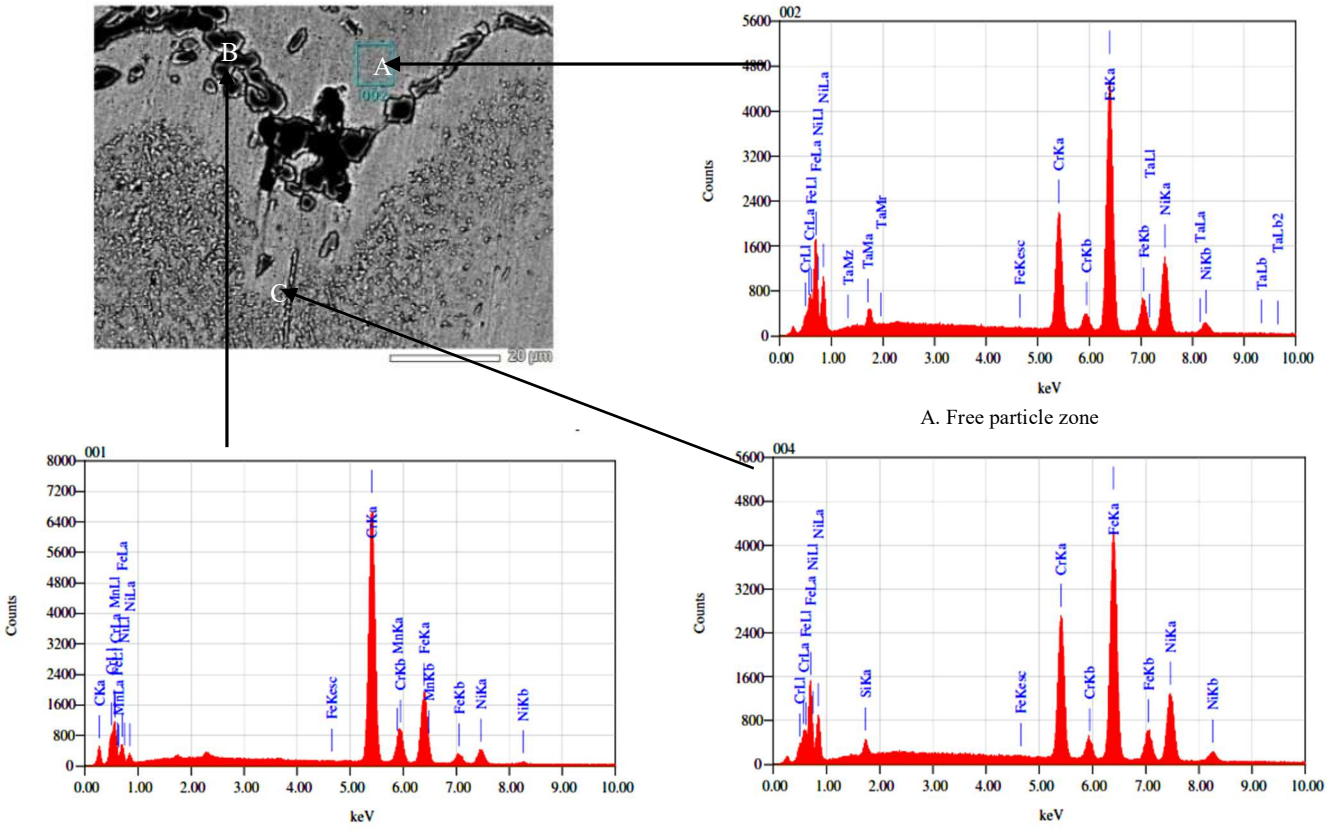


Fig. 5 SEM micrographs and EDS results for free particle zone, (Cr, Fe)7C3 island and particle of an intermetallic compound of FeCrNi in the ASS a) as-cast and b) annealed at 1078 °C

The hardness profile of ASS before and after annealed temperatures from 400 to 1078°C can be seen in Figure 6. The hardness of ASS as-cast is relatively low at around 163.9 HVN. This value increased after annealing at 400-800°C, from 188.08 to 196.51 HVN, and again decreased after annealing 950-1078°C, from 164.27 to 162.85 HVN. Dendritic structures, including interdendritic regions in the ASS formed before and after annealing up to 1078°C produce this hardness fluctuation.

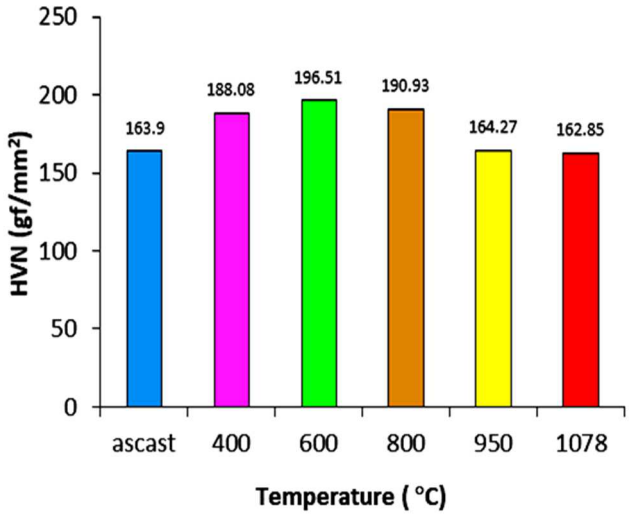


Fig. 6 Hardness profile of the ASS samples: as-cast and annealing at 400, 600, 800, 950, and 1078°C

The microstructure of ASS is composed of a dendrite structure as a matrix of γ-FeNi with fine particles of FeNiCr compound and eutectic structures of FeNiCr at the inter-dendrite region consisting of free particle zones and islands of $(Cr, Fe)_7C_3$. This structure is commonly formed in ASS and is a characteristic ASS castings structure reported by some studies [15-18]. Although the annealing temperature is increased from 400 to 1078°C, this structure still exists. The effect of annealing is seen in the changes in dendrite size and interdendritic region. There is a tendency to increase DAS with increasing annealing temperature. This change is possible because the temperature range for stable austenite is widened (Sheaffer diagram) due to austenite-forming elements such as Ni. Therefore, dendrites will enlarge at 950 and 1078 °C due to the development of energy being greater than the low annealing temperature. Also, carbide islands at the inter-dendrite region also enlarge with increasing annealing temperatures. Thus, microstructural formation during annealing occurs by enlarging the size of dendrites and carbide islands in the inter-dendrite region, as shown in figures 4.f and 5.c.

Hardness will decrease with the increasing of the grain size, including dendrites arm spacing of the material. Because in this study, the DAS formed at 1078°C were extensive compared to the DAS formed at a lower temperature of 950°C, followed by the DAS formed at 800, 600, and 400°C. Then, ASS's hardness after being annealed at 1078°C is the lowest hardness, 162.45 HVN which was successfully

observed in this study with DAS of 197.40 μm. The highest hardness that can be noted in the study amounted to 196.51 HVN with DAS of 62.11 μm. Moreover, small deformation, as indicated by low lattice parameter occurred in the ASS after annealed at 400, 600 and 800°C. Both the large size of DAS which has a low density of surfaces and small deformation in the crystal structure as barriers to deformation during hardness testing can contribute small effect so that the hardness of ASS annealed at 1078°C is lower as compared to the ASS annealed below 1078°C.

With the formation of $(Cr, Fe)_7C_3$ islands containing high C content, there is a free particle zone or the Cr-deflection zone around the island. This zone is a measurement of corrosion sensitivity for ASS. Since generally the Cr content limit for minimum sensitivity is 12% [16] while the Cr content in the particle-free zone is 16.36% Cr for ASS as-Cast and 17.45% Cr for ASS annealed at 1078°C, it is estimated that besides the matrix, the interdendritic region of ASS as-cast and annealed remains to have good corrosion resistance.

## IV. Conclusion

Based on the discussion about the microstructural formation of 15Cr-25Ni austenitic stainless steel cast before and after annealing at temperatures of 400, 600, 800, 950, and 1078°C for 30 minutes. It can be concluded as follows: microstructure of 15Cr-25Ni austenitic stainless steel cast before and after annealing consists of dendrite structures of austenite, γ-FeNi as a matrix and the eutectic structure of Fe-Ni-Cr as an interdendritic region, a matrix of γ-FeNi formed at low annealing temperatures of 400-800°C experiences more deformation as compared to high annealing temperatures of 950 and 1078°C, dendritic arm spacing in the matrix of 15Cr-25Ni austenitic stainless steel slightly fluctuates at annealing temperatures at 400-800°C and significantly increases at annealed temperatures of 950 and 1078°C, islands of $(Fe, Cr)_7C_3$ in the interdendritic region develops more massive when the annealing temperature increases to 1078°C and hardness profile of for 15Cr-25Ni austenitic stainless steel shows higher level after annealing at 400-800°C as compared to after annealing at 950 and 1078°C.

## Acknowledgment

The authors would like to extend their sincerest appreciation to Prof. Dr Ridwan, Head of Center for Science and Technology of Advanced Materials, to Dr Abu Khalid Rivai, Head of BSBM and Dr Iwan Sumirat, Head of BTBN BATAN, for their excellent supports and Coordination so this research can be finished properly.

## References

[1] Abdalla,A.M., Hossain,S., Petra,P.M., Ghasemi,M. Azad,A.K., Achievements and trends of solid oxide fuel cells in clean energy plane: a perspective review. Front. Energy 1-24, 2018. https://doi.org/10.1007/s11708-018-0546-2.

[2] Manal, A. S. Optimization of Multiple Effect Evaporators Designed for Fruit Juice Concentrate. Am. J. of Energy Eng. Special Issue: Energy Conservation in Food Industry. Vol. 3, No. 2-1, pp. 6-11, 2015. doi: 10.11648/j.ajee.s.2015030201.12.

[3] Setyawan, A. and Sujati, N. M., Evaluasi hasil analisis efisiensi kinerja sistem evaporator IPLR tahun 2014-2017, Prosiding Seminar Nasional Teknologi Pengelolaan Limbah XV, p. 255-259, 2017.

[4] Effendi,N. Darwinto, T., Parikin *et al.,* Indonesian J. of Mat. Sci. **15** 4, 187, 2014.

[5] Parikin, Dani, M., Sukaryo, S. G. 2019. Review on A New Austenitic 57Fe15Cr25Ni Stainless Steel at Temperature of 850°C for 30 Minutes Followed by Water Quenching Treatments. Malaysian Journal of Fundamental and Applied Sciences Vol.15, No.5, pp. 652-657.

[6] P.J.G. Nieto, V.M.G. Suárez, J.C.A. Antón *et al.,* Materials **8,** 3562, 2015.

[7] Parikin, Dani M., Jahja A.K., Iskandar R., Mayer J., Crystal Structure Investigation of Ferritic 73Fe24Cr2Si0.8Mn0.1Ni Steel for Multipurpouse Structural Material Applications, International Journal of Technology 1: 78-88, 2018.

[8] Parikin, Ismoyo, A.H., Iskandar, R., Dimyati, AMicrostructures and Hardness of TIG Welded Experimental 57Fe15Cr25Ni Steel, Makara Journal of Technology, University of Indonesia vol. 22/2, pp. 66-71, 2018.

[9] Parikin, Dani M., Ismoyo A.H., Dimyati A., Microstructures and Hardness of the Experimental 57Fe15Cr25Ni Austenitic Steel around the TIG Weld-Joints, Makara Journal of Technology-University of Indonesia, 22/2 66-67, 2018.

[10] L. Lutterotti, MAUD tutorial-instrumental Broadening Determination, Dipartimento di Ingegneria dei Materiali, Universita di Trento 38050 Trento, Italy, pp. 1-18, 2006.

[11] M. Kadziolka-Gawel, W. Zarek, E. Popiel and Chrobar, The Crystal Structure and Magnetic Properties of Selected fcc FeNi and Fe40Ni40B20 Alloys, Acta Physica Polonica A, 117 (2) 412-414, 2010.

[12] M.Dani, S. Mustopa, Parikin, Sumaryo, T. Sudiro, B. Hermant, D. R. Adhika, A. Dimyati, Syahbuddin, Sri Hardjanto, E. A. Basuki, C. A. Huang, Effect of Spark Plasma Sintering (SPS) at temperature of 900C and 950°C for 5 Minutes on Microstructural Formation of Fe-25Ni-17Cr Austenitic Stainless Steel, International Journal of Emerging Trends in Engineering Research, 8(8), 4845 – 4853, 2020.

[13] S. Mustopa, M.Dani, Parikin T. Sudiro, B. Hermanto, D. R. Adhika, Syahbuddin, C. A. Huang, Effect of Temperature of Spark Plasma Sintering on the Development of Oxide Compoundin the Fe-25Ni-17Cr Austenitic Stainless Steel, International Journal of Emerging Trends in Engineering Research, 8(9), 5661-5667, 2020.

[14] M. Dani, A. Dimiyanti, Parikin, D.R. Adhika, A.K. Jahja, A. Insani, Syahbuddin, C.A. Huang, Microstruture and Deformation of 57Fe17Cr25NiSi Austenitic Super Alloy After Arc Plasma Sintering, International Journal of Technology 10(5), 988-998, 2019.

[15] K. Wieczerzak, P. Bala, M. Stepien, G. Cios, T. Koziel, The Characterization of Cast Fe-Cr-C Alloy, Archives of Metallurgy and Materials, Volume 60 (2) 779-782, 2015.

[16] Majid Abbasi, Mahdich Yahdatnia and Ali Navael, Solidification Microstructure of HK Resistant Steel, International Journal of Metal Casting, 9(4), 19-26, 2015.

[17] Francisco J.G. Silva, Jorge Santos, and R. Gouveia, Dissolution of Grains Boundary Carbide by the Effect of Solution Annealing Heat Treatment and Aging Treatment on Heat-Resistant Cast Steel HK30, Metals 251(7), , 1-12, 2017.

[18] EA Kenik, J.T. Busby, D.T. Hoelzer, A.F. Rowecliffe, and J.M. Vitek, Microstructure and Elemental Distribution in a Cast Austenitic Steel, Microsc. Microanal. 13(2), 2007.